Material dependence of the wire-particle Casimir interaction

E. Noruzifar,[1] P. Rodriguez-Lopez,[2,3,4] T. Emig,[5] and R. Zandi[1]

[1]*Department of Physics and Astronomy, University of California, Riverside, California 92521, USA*

[2]*Departamento de Física Aplicada I and GISC, Facultad de Ciencias Físicas, Universidad Complutense, E-28040 Madrid, Spain*

[3]*Departamento de Matemáticas and GISC, Universidad Carlos III de Madrid, Avenida de la Universidad 30, E-28911 Leganés, Spain*

[4]*Department of Physics, Loughborough University, Loughborough LE11 3TU, United Kingdom*

[5]*Laboratoire de Physique Théorique et Modèles Statistiques, CNRS UMR 8626, Université Paris-Sud, F-91405 Orsay, France*

(Received 14 December 2012; published 8 April 2013)

We study the Casimir interaction between a metallic cylindrical wire and a metallic spherical particle by employing the scattering formalism. At large separations, we derive the asymptotic form of the interaction. In addition, we find the interaction between a metallic wire and an isotropic atom, both in the nonretarded and retarded limits. We identify the conditions under which the asymptotic Casimir interaction does not depend on the material properties of the metallic wire and the particle. Moreover, we compute the exact Casimir interaction between the particle and the wire numerically. We show that there is a complete agreement between the numerics and the asymptotic energies at large separations. For short separations, our numerical results show good agreement with the proximity force approximation.

DOI: 10.1103/PhysRevA.87.042504 PACS number(s): 31.30.jh, 03.70.+k

I. INTRODUCTION

Casimir forces contribute significantly to the effective interaction of micro- and nanometer-sized structures [1]. For identical objects or mirror symmetric configurations, this type of interaction is attractive [2] and can cause stiction in micromotors and other similar structures [3]. More generally, if the permittivities of the objects are higher or lower than those of the surrounding medium, any equilibrium position of the objects is unstable due to the Casimir interactions [4]. Therefore, a good quantitative understanding of such forces is a key parameter in the design and manufacturing of micromechanical devices.

It is important to study the Casimir forces for different shapes as they strongly depend on the geometry and material properties [1,5,6]. Technically, investigating the interplay between the shape and material effects is quite involved. The scattering formalism provides a powerful tool to calculate the Casimir interaction between objects of general shape and material properties [7,8]. There is much recent research activity based on the scattering formalism, e.g., for edges and tips [9,10], anisotropic particles [11], wires and plates [12–15], spheres and plates [16], and periodic structures [17–19]. For some further recent examples, see Ref. [20].

An important geometry which has not yet been investigated in detail consists of a wire and a particle (atomic or macroscopic). In the plane-particle geometry this force is known as the Casimir-Polder (CP) interaction [21]. Our study of the wire-particle case is motivated by theories [22] and experiments [23,24] on the two-dimensional quantum scattering of neutral atoms or molecules at wires or nanotubes. In an early work, the interaction between a filament and an isotropic atom has been studied for perfectly and nonperfectly conducting metals [25]. Later, Eberlein and Zietal studied the interaction between a neutral atom and a perfect metal cylinder, using perturbation theory [26,27]. Recently, the Casimir energy for a polarizable microparticle and an ideal metal cylindrical shell has been computed using the Green's function technique [28]. The focus of previous studies was mainly on the interaction between a metal wire and a perfect metal particle or an atom. Therefore, the influence of material properties of the spherical particles on the energy remains to be studied in detail.

In this work, we study the Casimir interaction between a metallic spherical particle and cylindrical metallic wire where the latter is described by the Drude, plasma, or perfect metal model. Using the scattering formalism, we derive a general expression for the Casimir interaction between the particle and cylinder. From this general expression we determine the behavior of the Casimir energy in various limiting cases (separation regimes) analytically, and numerically over a wide range of separations. Interestingly, we find ranges of distances in which the Casimir interaction does not depend on the material properties of the metallic wire. In contrast, we find that the interaction depends in general on the material properties of the metallic particle at all separations. An exception is the plasma sphere with a plasma wavelength that is much smaller than the size of the sphere for which the Casimir interaction is universal at asymptotically large distances. At short separations, we compute the exact Casimir interaction numerically and compare it both with the asymptotic results and the prediction of proximity force approximation (PFA). In both limits we obtain good agreement.

The structure of the rest of the paper is as follows: In Sec. II, we review the scattering approach and derive the elements that are needed for computing the interaction between a wire and a particle. In Sec. III, the large-distance asymptotic interaction between a metallic wire and a particle (metal sphere and isotropic atom) is derived for the perfect metal, plasma, and Drude models. In Sec. IV, the exact Casimir interaction is computed numerically and compared with the asymptotic expansions. Section V is dedicated to the interaction at short separations where the PFA is expected to become reliable.

II. METHOD

We consider a cylindrical wire separated by a distance d from a spherical particle. We use the scattering formalism to

calculate the Casimir energy between the cylinder and sphere [7]. In general, the Casimir free energy between two objects at the temperature T is given by

$$\mathcal{E} = k_B T {\sum_{n=0}^{\infty}}' \ln\det[\mathbf{1} - \mathbb{N}(\kappa_n)], \tag{1}$$

where $\mathbf{1}$ is the identity matrix, κ_n is the Matsubara wave number $\kappa_n = 2\pi n k_B T/\hbar c$, and the matrix $\mathbb{N}$ factorizes into the scattering amplitudes (T matrices) as well as translation matrices which describe the coupling between the multipoles on distinct objects. The primed sum denotes that the contribution of $n = 0$ has to be weighted by a factor of $1/2$.

At zero temperature, the primed sum in Eq. (1) is replaced by an integral along the imaginary frequency axis,

$$\mathcal{E} = \frac{\hbar c}{2\pi}\int_0^{\infty} d\kappa \ln\det(\mathbf{1} - \mathbb{N}), \tag{2}$$

with κ the Wick-rotated frequency. The elements of the matrix $\mathbb{N}$ for electric (E) and magnetic (M) polarizations ($\alpha,\beta,\gamma = E,M$) and cylindrical wave functions m and m' are

$$\mathbb{N}^{\alpha\beta}_{k_z m,k_z' m'} = \sum_{\gamma=E,M}\sum_{m''=-\infty}^{\infty} T^{\alpha\gamma}_{\mathrm{s},k_z m,k_z' m''} \sum_{n=-\infty}^{\infty} \mathcal{U}^{\mathrm{sc}}_{k_z' m'' n} T^{\gamma\beta}_{\mathrm{c},k_z' n} \mathcal{U}^{\mathrm{cs}}_{k_z' n m'}, \tag{3}$$

where k_z is the wave number along the z axis, and T_{c} and T_{s} are the T matrices of the cylinder and sphere in cylindrical basis, respectively. The translation matrix $\mathcal{U}^{\mathrm{sc}}$ relates regular cylindrical vector waves to outgoing ones.

The translation matrices do not couple different polarizations, and for both E and M polarizations their matrix elements are given by

$$\mathcal{U}^{\mathrm{sc}}_{nn'} = (-1)^{n'} K_{n-n'}(pd), \quad \mathcal{U}^{\mathrm{cs}}_{nn'} = (-1)^{n-n'} \mathcal{U}^{\mathrm{sc}}_{nn'}, \tag{4}$$

where $p = \sqrt{\kappa^2 + k_z^2}$ and $K_n(x)$ is the modified Bessel function of the second kind. Note that the $\mathbb{N}$-matrix elements in Eq. (3) are written in a cylindrical basis to avoid the complicated form of the translation matrices in the spherical basis [7].

The T matrix of the sphere in the cylindrical basis is derived in Appendix B and is given by

$$T^{\alpha\gamma}_{\mathrm{s},k_z m,k_z' m} = \frac{1}{2\pi\kappa L}\sum_{\ell=\max(1,|m|)}^{\infty}\sum_{\beta}(1 - 2\delta_{\alpha,\beta}) \times D^{\dagger}_{k_z m\alpha,\ell m\beta} T^{\beta}_{\mathrm{s},\ell m} D_{\ell m\beta,k_z' m\gamma}, \tag{5}$$

where L is the length of the cylinder, ℓ is the quantum number of the spherical electromagnetic waves, $\beta = E,M$ is the electromagnetic polarization, and D is the conversion matrix from the cylindrical to spherical basis. The elements of the conversion matrix are given in Appendix C. Note that in Eq. (5), $T^{\beta}_{\mathrm{s},\ell m}$ is the T matrix of the sphere in the spherical basis.

To obtain the Casimir energy from Eq. (2), we plug Eqs. (4) and (5) into (3) and use the identity $\det(\mathbf{1} - \mathbf{AB}) = \det(\mathbf{1} - \mathbf{BA})$. The $\mathbb{N}$ matrix for the energy between the sphere and the cylinder is rewritten as

$$\mathbb{N}^{\alpha\beta}_{\ell m,\ell' m'} = \frac{1}{4\pi^2\kappa}\sum_{\gamma,\gamma'} T^{\alpha}_{\mathrm{s},\ell m}\int_{-\infty}^{\infty} dk_z D_{\ell m\alpha,k_z m\gamma} \times \tilde{\mathbf{T}}^{\gamma\gamma'}_{mm'} D^{\dagger}_{k_z m'\gamma',\ell' m'\beta}(1 - 2\delta_{\beta,\gamma'}), \tag{6}$$

with

$$\tilde{\mathbf{T}}^{\gamma\gamma'}_{mm'} = \sum_{n=-\infty}^{\infty} \mathcal{U}^{\mathrm{cs}}_{k_z mn\gamma} T^{\gamma\gamma'}_{\mathrm{c},k_z n} \mathcal{U}^{\mathrm{sc}}_{k_z nm'\gamma'}. \tag{7}$$

In this work, to study the impact of the material properties of the metallic objects on the Casimir interaction, we employ the plasma, Drude, and perfect metal dielectric properties with the constant magnetic permeability $\mu = 1$. The Drude model dielectric response is given by

$$\epsilon(ic\kappa,\lambda_{\mathrm{p}},\lambda_\sigma) = 1 + \frac{(2\pi)^2}{(\lambda_{\mathrm{p}}\kappa)^2 + \lambda_\sigma\kappa/2}, \tag{8}$$

where λ_{p} is the plasma wavelength and $\lambda_\sigma = 2\pi c/\sigma$ is the length scale associated with the conductivity σ. Equation (8) reproduces the plasma model dielectric function for $\lambda_\sigma = 0$. Note that the material properties of the sphere and the cylinder enter into the calculations through the T matrices (see Appendix A).

III. LARGE-SEPARATION REGIME: ASYMPTOTIC CASIMIR ENERGY

In this section, we study the large-separation asymptotic behavior of the Casimir interaction between a particle and a wire. We consider a spherical particle with radius R_{s} and a cylindrical wire with radius R_{c}. In order to find the large-distance ($d \gg R_{\mathrm{c}}, R_{\mathrm{s}}$) asymptotic form of the Casimir interaction, one has to find the behavior of the T matrices in the low-frequency limit.

A. Asymptotic behavior of T matrices

1. *T matrix of a wire*

In this section, we obtain the asymptotic form of the T-matrix elements of a wire at large separations. Using the dielectric function given in Eq. (8), we find the T-matrix element of the wire for E polarization and $n = 0$ at small frequencies ($\kappa \ll 1, k_z/\kappa$ fixed) is

$$T_0^{EE} \approx -\frac{p^2}{C(\kappa) - p^2\ln(pR_{\mathrm{c}})}, \tag{9}$$

where $p = \sqrt{\kappa^2 + k_z^2}$. The parameter $C(\kappa)$ depends on the dielectric properties of the wire. For a perfect metal wire $C(\kappa) = 0$ and for a plasma wire with the plasma wavelength λ_{p}, $C(\kappa) \approx \lambda_{\mathrm{p}}^2\kappa^2/(2\pi^2 R_{\mathrm{c}}^2)$ if the plasmon oscillations cannot build up transverse to the wire axis as the diameter is too small, i.e., $R_{\mathrm{c}} \ll \lambda_{\mathrm{p}}$. In the opposite limit we approximately reproduce the T matrix of a perfect metal wire, i.e., $C(\kappa) \approx 0$. For a Drude wire with the conductivity σ and the characteristic length λ_σ, $C(\kappa) = \lambda_\sigma\kappa/(4\pi^2 R_{\mathrm{c}}^2)$ if $\kappa \ll \lambda_\sigma/\lambda_{\mathrm{p}}^2, 1/\lambda_\sigma$. The first condition ($\kappa \ll \lambda_\sigma/\lambda_{\mathrm{p}}^2$) means that the Drude behavior dominates over the plasma behavior, equivalent to the fact that in the dominator of Eq. (8), the first term is much smaller than the second

one. The second condition ($\kappa \ll 1/\lambda_\sigma$) ensures that the Drude dielectric function is much larger than one, i.e., the metallic behavior is dominant [12,13].

At large separations, T_0^{EE} elements dominate over the other T-matrix elements since $T_0^{EM} = T_0^{ME} = 0$, $T_0^{MM} \sim \kappa^2$, and for $n \neq 0$ partial waves $T_n \sim \kappa^{2|n|}$. Note that for Drude cylinders $T_0^{EE} \sim \kappa$ while for plasma and perfect metal cylinders $T_0^{EE} \sim 1$.

2. *T matrix of a particle*

The T-matrix elements of a spherical particle have a different scaling compared to the ones for the cylindrical wire. For the plasma and perfect metal spheres $T_{s,\ell m} \sim \kappa^{2\ell+1}$. For Drude spheres the T-matrix elements for the electric E and magnetic M polarizations scale differently: $T^M_{s,\ell m} \sim \kappa^{2(\ell+1)}$ and $T^E_{s,\ell m} \sim \kappa^{2\ell+1}$. Therefore, the asymptotic behavior of the T matrix at large separations is dominated by the $\ell = 1$ elements. The asymptotic form of the T-matrix elements for the magnetic polarization M and $\ell = 1$ depends on the material properties of the sphere. While for a perfect metal sphere we have

$$T^M_{s,1m} \approx -\kappa^3 R_s^3/3, \tag{10}$$

for a plasma sphere with the plasma wavelength λ'_p we obtain

$$T^M_{s,1m} \approx -\frac{1}{3}\frac{I_{\frac{5}{2}}(2\pi R_s/\lambda'_p)}{I_{\frac{1}{2}}(2\pi R_s/\lambda'_p)}\kappa^3 R_s^3. \tag{11}$$

Note that in the limit of perfect conductivity $\lambda'_p \to 0$, we reproduce Eq. (10).

For a Drude sphere with the conductivity σ' and the characteristic length λ'_σ,

$$T^M_{s,1m} \approx -\frac{8\pi^2}{45}\frac{R_s}{\lambda'_\sigma}\kappa^4 R_s^4. \tag{12}$$

However, the asymptotic form of the T-matrix elements for E polarization and $\ell = 1$, up to the leading order, does not depend on the material properties, and is the same for the perfect metal, plasma, and Drude models,

$$T^E_{s,1m} \approx \tfrac{2}{3}\kappa^3 R_s^3. \tag{13}$$

Note that for the Drude sphere $T^M_{s,1m} \sim \kappa^4$, and thus we add the subleading term to the expansion of $T^E_{s,1m}$ in Eq. (13) and obtain

$$T^E_{s,1m} \approx \frac{2}{3}\kappa^3 R_s^3 - \frac{1}{4\pi^2}\frac{\lambda'_\sigma}{R_s}\kappa^4 R_s^4, \tag{14}$$

where the subleading term contains the material properties of the Drude wire.

3. *T matrix of an atom*

The above approach can also be used to calculate the Casimir energy between an atom and a wire. To this end, we consider a neutral two-level atom in the ground state, with the transition frequency ω_{10} [21]. We assume that the distance from the atom to the wire d is much larger than the radius of the wire R_c, i.e., $d/R_c \gg 1$. Moreover, we assume that the atom is isotropic and does not have magnetic polarizability. In the isotropic-dipole approximation, the only nonzero element of the T matrix reads

$$T^E_{\text{atom},1m} \approx \tfrac{2}{3}\alpha^E(\kappa)\kappa^3, \tag{15}$$

where α^E, the electric polarizability, is given by

$$\alpha^E(\kappa) = \frac{\alpha_0}{1+\kappa^2 d_{10}^2}, \tag{16}$$

with $d_{10} = c/\omega_{10}$, $\alpha_0 = f_{10}e^2/(m\omega_{10}^2)$, e the electron charge, m the mass, and f_{10} the oscillator strength of the $0 \to 1$ transition.

B. Asymptotic energy expression

In this section, using the asymptotic T-matrix expressions and Eq. (6), we derive the Casimir energy at large separations. Considering $\ln\det \equiv \mathrm{Tr}\ln$, we expand the integrand in Eq. (2) in powers of $\mathbb{N}$ for $\kappa \ll 1$ and k_z/κ fixed and find

$$\mathcal{E} \approx -\frac{\hbar c}{2\pi}\int_0^\infty d\kappa\, \mathrm{Tr}\,\mathbb{N}. \tag{17}$$

As discussed above, in the limit $d \gg R_s, R_c$ only the $\ell = 1$ terms contributes to the sphere T matrix, $T_{s,\ell m}$. Therefore, only the partial wave numbers $m = 0, \pm 1$ have to be taken into account to obtain the matrix $\mathbb{N}$. Using Eq. (6), we find

$$\begin{aligned}\mathrm{Tr}\,\mathbb{N} &\approx \sum_\gamma \sum_{m=-1}^{1} \tilde{\mathbb{N}}^{\gamma\gamma}_{1m,1m} \\ &= \frac{1}{4\pi^2\kappa}\sum_\gamma \sum_{m=-1}^{1} T^\gamma_{s,1m}\int_{-\infty}^{\infty} dk_z \tilde{D}_{1m\gamma,k_z mE}\tilde{\mathbf{T}}^{EE}_{mm} \\ &\quad \times \tilde{D}^{\mathrm{T}}_{k_z mE,1m\gamma}(1-2\delta_{\gamma,E}),\end{aligned} \tag{18}$$

with $\tilde{\mathbf{D}}$ the modified conversion matrix with real elements. The modified conversion matrix is related to the original one by $\mathbf{D}_{\ell m,k_z m} = (-1)^{\ell-m}(-i)^{\ell+m-1}\tilde{\mathbf{D}}_{\ell m,k_z m}$ (see Appendix C). Furthermore, the matrix $\tilde{\mathbf{T}}^{EE}_{mm}$ in Eq. (18) is equal to

$$\tilde{\mathbf{T}}^{EE}_{mm} \approx K_m^2(pd)T^{EE}_{c,k_z 0}. \tag{19}$$

Note that in Eq. (19), $T^{EE}_{c,k_z\pm 1}$ are neglected as they scale with higher powers of κ.

Inserting Eq. (19) into Eq. (18) and performing the sums, we find

$$\begin{aligned}-\mathrm{Tr}[\tilde{\mathbb{N}}] \approx \frac{1}{4\pi^2\kappa}\int_{-\infty}^{\infty} dk_z\, T^{EE}_{c,k_z 0} \\ \times\big[K_0^2(pd)\big(\tilde{D}^2_{10E,k_z 0M}T^M_{s,1} - \tilde{D}^2_{10M,k_z 0M}T^E_{s,1}\big) \\ + 2K_1^2(pd)\big(\tilde{D}^2_{11E,k_z 1M}T^M_{s,1} - \tilde{D}^2_{11M,k_z 1M}T^E_{s,1}\big)\big].\end{aligned} \tag{20}$$

The modified conversion matrix elements in Eq. (20) are (see Appendix C for all details)

$$\begin{aligned}&\tilde{D}_{10E,k_z 0M} = 0, \quad \tilde{D}_{10M,k_z 0M} = \sqrt{6\pi}\big(1+k_z^2/k^2\big)^{1/2}, \\ &\tilde{D}_{11E,k_z 1M} = \sqrt{3\pi}, \quad \tilde{D}_{11M,k_z 1M} = \sqrt{3\pi}k_z/k.\end{aligned} \tag{21}$$

Inserting Eq. (21) into Eq. (20) and using the leading term in the $T^E_{s,1m}$ expansion, we find the asymptotic energy between a perfect metal, plasma, and Drude cylinder and a spherical particle or an atom. Using Eq. (17) and the T-matrix expansions

up to κ^3 [see Eqs. (10)–(14)], we obtain the general expression for the asymptotic energy

$$\frac{\mathcal{E}}{\hbar c} \approx \frac{1}{\pi^2}\int_0^\infty d\kappa \int_0^\infty dk_z T_{\mathrm{c},0}^{EE} \times \chi\left[p^2 K_0^2(pd) + \left(2\Lambda_0\kappa^2 + k_z^2\right)K_1^2(pd)\right], \quad (22)$$

with $\chi = R_\mathrm{s}^3$ for the spherical particle and $\chi = \alpha^E(\kappa)$ for the isotropic atom. Moreover, Λ_0 is proportional to $T_{\mathrm{s},1}^M$ [see Eq. (20)], with $\Lambda_0 = 1/4$ for the perfect metal particle, $\Lambda_0 = I_{\frac{5}{2}}(2\pi R_\mathrm{s}/\lambda_\mathrm{p}')/[4I_{\frac{1}{2}}(2\pi R_\mathrm{s}/\lambda_\mathrm{p}')]$ for the plasma particle, and $\Lambda_0 = 0$ for the atom and the Drude particle. The latter is due to the fact that $T_{\mathrm{s},1}^M$ is set to zero in Eq. (22). $T_{\mathrm{s},1}^M$ for the atom is indeed zero and for the Drude particle scales with κ^4 [see Eq. (12)]. Therefore, for the Drude particle the asymptotic energy given by Eq. (22) needs a correction because of the κ^4 terms in Eqs. (12) and (14), which is

$$\frac{\delta\mathcal{E}_\mathrm{DS}}{\hbar c} = \frac{1}{\pi^2}\int_0^\infty \kappa\, d\kappa \int_0^\infty dk_z T_{\mathrm{c},0}^{EE} \chi\left[\frac{3\lambda_\sigma'}{8\pi^2}p^2 K_0^2(pd) + \left(\frac{3\lambda_\sigma'}{8\pi^2}k_z^2 - \frac{4\pi^2 R_s^2}{15\lambda_\sigma'}\kappa^2\right)K_1^2(pd)\right]. \quad (23)$$

Inserting Eq. (9) into Eq. (22) and using the polar coordinates, $\kappa \to \rho\cos(\theta)/d$ and $k_z \to \rho\sin(\theta)/d$, we find

$$\frac{\mathcal{E}}{\hbar c} \approx -\frac{1}{\pi^2 d^4 \ln(2d/R_\mathrm{c})}\int_0^\infty d\rho\rho^3 \int_0^{\pi/2}\frac{d\theta}{1+C(\rho,\theta)} \times \chi\left\{K_0^2(\rho) + [\sin^2(\theta) + 2\Lambda_0\cos^2(\theta)]K_1^2(\rho)\right\}, \quad (24)$$

where for the perfect metal cylinder $C(\rho,\theta) = 0$, for the plasma cylinder $C(\rho,\theta) \approx \xi\cos^2(\theta)$ with $\xi = \lambda_\mathrm{p}^2/[2\pi^2 R_\mathrm{c}^2\ln(2d/R_\mathrm{c})]$, and for the Drude cylinder $C(\rho,\theta) = \xi'\cos(\theta)/\rho$ with $\xi' = \lambda_\sigma d/[4\pi^2 R_\mathrm{c}^2\ln(2d/R_\mathrm{c})]$.

The correction $\delta\mathcal{E}_\mathrm{DS}$ for the Drude particle in polar coordinates (ρ,θ) reads

$$\frac{\delta\mathcal{E}_\mathrm{DS}}{\hbar c} = \frac{3R_\mathrm{s}^3\lambda_\sigma'}{8\pi^4 d^5\ln(2d/R_\mathrm{c})}\int_0^\infty \rho^4\, d\rho\int_0^{\pi/2} d\theta\frac{\cos(\theta)}{1+C(\rho,\theta)} \times\left[K_0^2(\rho) + \left(\sin^2(\theta) - \frac{32\pi^4 R_s^2}{45\lambda_\sigma'^2}\cos^2(\theta)\right)K_1^2(\rho)\right]. \quad (25)$$

Now we use Eqs. (24) and (25) for different material properties and calculate the Casimir interaction for various limiting cases.

C. The Casimir interaction between a wire and a spherical particle

Below we present the large-separation asymptotic energies between a metallic spherical particle and a metallic wire.

1. The perfect metal wire

For a perfect metal wire and a perfect metal, plasma, or Drude particle, the energy integral in Eq. (24) results in

$$\frac{\mathcal{E}}{\hbar c} \approx -\frac{\Lambda_0+1}{3\pi}\frac{R_\mathrm{s}^3}{d^4\ln(2d/R_\mathrm{c})}. \quad (26)$$

It is important to note that Eq. (26) depends on the material properties of the spherical particle through the quantity Λ_0. For a perfect metal wire and a plasma particle, in the limiting case of small plasma wavelengths, $\lambda_\mathrm{p}' \ll R_\mathrm{s}$, we reproduce the perfect conductivity form with $\Lambda_0 \approx 1/4$. In the limit of large plasma wavelengths, $\lambda_\mathrm{p}' \gg R_\mathrm{s}$, we obtain $\Lambda_0 \approx \pi^2 R_\mathrm{s}^2/(15\lambda_\mathrm{p}'^2)$. Since $\Lambda_0 \ll 1$, the plasma wavelength of the spherical particle does not have a significant contribution to the asymptotic energy.

For the Drude particle, using Eq. (25), the correction to the asymptotic energy given by Eq. (26) reads

$$\frac{\delta\mathcal{E}_\mathrm{DS}}{\hbar c} = -\frac{R_\mathrm{s}^3}{32d^5\ln(2d/R_\mathrm{c})}\left(\frac{\pi^2 R_\mathrm{s}^2}{2\lambda_\sigma'} - \frac{63\lambda_\sigma'}{64\pi^2}\right), \quad (27)$$

and scales with d^{-5}. Depending on the terms in the parentheses, this correction can have a significant contribution to the asymptotic energy. In the limit of high conductivity, $\lambda_\sigma' \ll R_\mathrm{s}$, the first term in the parentheses dominates over the second one. For this specific case, if $\lambda_\sigma' d \ll R_\mathrm{s}^2$, the correction becomes even larger than the asymptotic energy itself, i.e., $\delta\mathcal{E}_\mathrm{DS} \gg \mathcal{E}$.

Note that in Eq. (27), the second term in the parentheses dominates only at low conductivity limit $\lambda_\sigma' \gg R_\mathrm{s}$ in which the spherical particle is considered to be a very poor conductor. In general, the second term does not have a noticeable contribution to the asymptotic energy for good conductors such as copper and gold.

2. The plasma wire

For a plasma wire and a plasma or a perfect metal particle, the polar and radial integrals in Eq. (24) can easily be performed,

$$\frac{\mathcal{E}}{\hbar c} \approx -\frac{R_\mathrm{s}^3}{\pi d^4\ln(2d/R_\mathrm{c})}f(\xi), \quad (28)$$

with

$$f(\xi) = \frac{1}{3\xi}(2\Lambda_0 - 1)[1-(1+\xi)^{-\frac{1}{2}}] + \frac{1}{2}(1+\xi)^{-\frac{1}{2}}, \quad (29)$$

where ξ is given below Eq. (24), $\xi = \lambda_\mathrm{p}^2/[2\pi^2 R_\mathrm{c}^2\ln(2d/R_\mathrm{c})]$. In the small plasma wavelength limit, $\lambda_\mathrm{p}/R_\mathrm{c} \ll \sqrt{\ln(2d/R_\mathrm{c})}$, we reproduce the perfect metal wire results given by Eqs. (26) and (27).

In the opposite limit $\lambda_\mathrm{p}/R_\mathrm{c} \gg \sqrt{\ln(2d/R_\mathrm{c})}$, the asymptotic energy reads

$$\frac{\mathcal{E}}{\hbar c} \approx -\frac{R_\mathrm{c}R_\mathrm{s}^3}{\lambda_\mathrm{p}d^4}\left(\frac{1}{\sqrt{2\ln(2d/R_\mathrm{c})}} + \frac{4\pi\Lambda_0}{3}\frac{R_\mathrm{c}}{\lambda_\mathrm{p}}\right). \quad (30)$$

For a perfect metal spherical particle, $\Lambda_0 = 1/4$, and the second term can be neglected as we are at the large plasma wavelength regime.

For a plasma spherical particle with plasma wavelength λ_p', if $\lambda_\mathrm{p}' \ll R_\mathrm{s}$, $\Lambda_0 \approx 1/4$ and the energy is the same as in the case of a perfect particle and a plasma wire. In the opposite limit $\lambda_\mathrm{p}' \gg R_\mathrm{s}$, we have $\Lambda_0 \approx \pi^2 R_\mathrm{s}^2/(15\lambda_\mathrm{p}'^2) \ll 1$ and the plasma wavelength of the particle does not have a significant effect

on the asymptotic energy, and the asymptotic energy is mainly dominated by the material properties of the plasma wire.

For a Drude particle, the asymptotic energy is given by Eq. (30), together with a correction obtained by Eq. (25). The correction reads

$$\frac{\delta\mathcal{E}_{\rm DS}}{\hbar c}=-\frac{3}{64}\frac{R_{\rm s}^3}{d^5}\left(\frac{R_{\rm c}}{\lambda_{\rm p}}\right)^2\left[\frac{9}{4}\left(\frac{5}{8}-\ln 2\right)\lambda'_\sigma+\pi^4\frac{R_{\rm s}^2}{\lambda'_\sigma}\right]. \tag{31}$$

Since for good conductors $\lambda'_\sigma \ll R_{\rm s}$, similar to the case of a perfect metal wire, the second term dominates over the first one.

3. The Drude wire

For a Drude wire and a perfect metal or plasma particle, in the limit $\xi' \ll 1$ or $d^2/R_{\rm c}^2 \ll d/\lambda_\sigma$, using Eqs. (24) and (25), we reproduce the perfect metal wire results [see Eqs. (26) and (27)].

In the opposite limit, $\xi' \gg 1$ or equivalently $d^2/R_{\rm c}^2 \gg d/\lambda_\sigma$ and $d \gg \lambda_{\rm p}^2/\lambda_\sigma$, the integrations in Eq. (24) result in

$$\frac{\mathcal{E}}{\hbar c}\approx-\frac{9\pi^2}{64}\frac{R_{\rm s}^3R_{\rm c}^2}{\lambda_\sigma d^5}\left[5\Lambda_0+4\ln\left(\lambda_\sigma d/R_{\rm c}^2\right)\right]. \tag{32}$$

For a perfect metal particle, $\Lambda_0 = 1/4$, and the energy given by Eq. (32) is always attractive since $\lambda_\sigma d \gg R_{\rm c}^2$.

For the plasma particle, in the limit of small plasma wavelength $\lambda'_{\rm p} \ll R_{\rm s}$, $\Lambda_0 \approx 1$, and the particle behaves as a perfect metal. In the opposite limit, $\lambda'_{\rm p} \gg R_{\rm s}$, as previously seen, we find $\Lambda_0 \approx \pi^2 R_{\rm s}^2/(15\lambda_{\rm p}'^2)$. In this case the second term in Eq. (32) dominates, which means that the material properties of the plasma particle do not have a significant effect on the asymptotic Casimir energy.

Under the same condition $\xi' \gg 1$, using Eq. (25), the correction to Eq. (32) reads

$$\frac{\delta\mathcal{E}_{\rm DS}}{\hbar c}=-\frac{R_{\rm c}^2R_{\rm s}^3\ln(2d/R_{\rm c})}{\lambda_\sigma d^6}\left(\frac{32\pi^3R_{\rm s}^2}{25\lambda'_\sigma}-\frac{7\lambda'_\sigma}{5\pi}\right). \tag{33}$$

As discussed above, for metallic particles, the second term in Eq. (33) is much smaller than the first one.

D. The Casimir energy between a wire and an atom

We calculate the Casimir energy between a wire and an atom in both retarded and nonretarded limits. To find the asymptotic energies at large separations, we use Eq. (24) with $\Lambda_0 = 0$.

1. The retarded limit

In the retarded limit, $d \gg d_{10}$, we find the Casimir energy between a perfect metal wire and an atom as

$$\frac{\mathcal{E}}{\hbar c}\approx-\frac{1}{3\pi}\frac{\alpha_0}{d^4\ln(2d/R_{\rm c})}. \tag{34}$$

Equation (34) is in complete agreement with the results in Refs. [25–28]. It is important to note that even though the asymptotic energies for an atom given in Eq. (34) and for a perfect metal particle given in Eq. (26) have the same scaling behavior, the numerical coefficients do not match: $1/(3\pi)$ for the atom and $5/(12\pi)$ for the spherical particle. This discrepancy is due to the lack of magnetic polarizability in the isotropic atoms.

For the plasma wire and an atom in the limit $\xi \gg 1$ or equivalently $\lambda_{\rm p}/R_{\rm c} \gg \sqrt{\ln(2d/R_{\rm c})}$ and $d \gg d_{10}$, the asymptotic energy reads

$$\frac{\mathcal{E}}{\hbar c}\approx-\frac{R_{\rm c}}{\lambda_{\rm p}}\frac{\alpha_0}{d^4\sqrt{2\ln(2d/R_{\rm c})}}, \tag{35}$$

which is in agreement with the atom-plasma wire result in Ref. [25]. In the limit $\lambda_{\rm p}/R_{\rm c} \ll \sqrt{\ln(2d/R_{\rm c})}$ and $d \gg d_{10}$, we reproduce the perfect metal wire-atom interaction energy given in Eq. (34).

For the Drude wire and an atom, in the region of intermediate distances $\xi' \gg 1$ or equivalently $d/R_{\rm c} \gg R_{\rm c}/\lambda_\sigma$, in the retarded limit $d \gg d_{10}$, the asymptotic energy reads

$$\frac{\mathcal{E}}{\hbar c}\approx-\frac{9\pi^2}{16}\frac{\alpha_0R_{\rm c}^2}{\lambda_\sigma d^5}\ln\left(\lambda_\sigma d/R_{\rm c}^2\right). \tag{36}$$

Equation (36) is in agreement with Ref. [25]. In the opposite limit, $\xi' \ll 1$ or $d/R_{\rm c} \ll R_{\rm c}/\lambda_\sigma$ and $d \gg d_{10}$, once again we reproduce the perfect metal wire-atom asymptotic interaction energy [see Eq. (34)].

2. The nonretarded limit

In the nonretarded limit, $d \ll d_{10}$, using Eq. (24) with $\Lambda_0 = 0$, we perform the angular integral for the perfect metal, plasma, and Drude wires.

For the perfect metal wire, the radial integral can easily be obtained. Expanding the result of the integral for $d \ll d_{10}$ yields

$$\frac{\mathcal{E}}{\hbar}\approx-\frac{\pi}{16}\frac{\alpha_0\,\omega_{10}}{d^3\ln(2d/R_{\rm c})}. \tag{37}$$

For the plasma wire, the radial integral over ρ in Eq. (24) cannot readily be performed in the nonretarded limit. Therefore, we expand the integrand for $d/d_{10} \ll 1$. In the limit $d \ll R_{\rm c}d_{10}/\lambda_{\rm p}$ the expansion of the integrand does not depend on the material properties up to the leading order. Therefore, performing the integration over ρ results in the perfect metal wire-atom interaction energy given in Eq. (37).

Similar to the plasma wire, the radial integration in Eq. (24) is not easily calculable for the Drude wire. Analogously, we expand the integrand for $d/d_{10} \ll 1$ and then perform the integral over ρ. In the limit $d \ll R_{\rm c}\sqrt{d_{10}/\lambda_\sigma}$, we find Eq. (37) for a perfect metal wire and an atom. This is due to the fact that the material properties of the Drude wires do not play any role at intermediate separations (see Refs. [12,13]).

E. Universality

In previous sections, we have derived the asymptotic energies between a metallic wire and a metallic spherical particle for different dielectric properties, described by the Drude, plasma, or perfect metal models. We have found that in all cases, the Casimir energy depends on the material properties of the spherical particle. This is due to the fact that the material property of a sphere has a significant contribution to its T matrix [16]. In contrast, for parallel metallic wires and a wire-plate geometry, at intermediate distances, the asymptotic

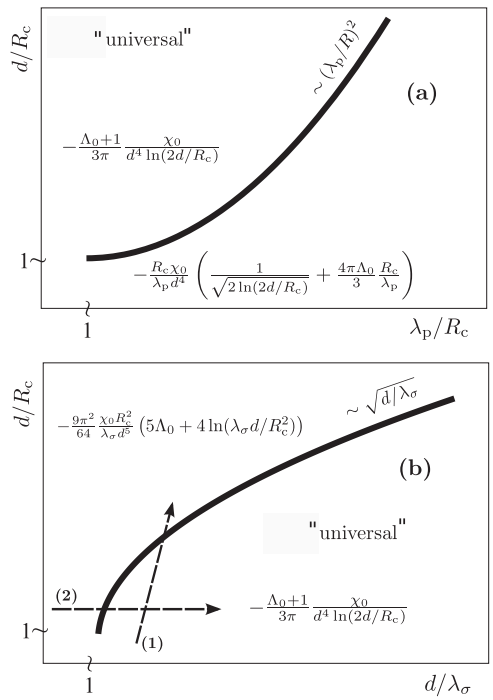

FIG. 1. Interaction between a wire and a particle and between a wire and an atom in the retarded limit. The formulas describe the rescaled interaction energies $\mathcal{E}/(\hbar c)$. The parameter $\chi_0 = \alpha_0$ for the atom and $\chi_0 = R_s^3$ for the particle. (a) Interaction between a plasma wire and a metallic spherical particle. The asymptotic results correspond to the regimes sufficiently far from the curve $\ln(d/R_c) \sim (\lambda_p/R_c)^2$ and for $d/R_c, \lambda_p/R_c \gg 1$. (b) Interaction between a Drude wire and a metallic particle. The separating curve is given, up to logarithmic corrections, by $d/R_c \sim \sqrt{d/\lambda_\sigma}$. The energy expressions hold for $d/R_c, d/\lambda_\sigma \gg 1$, and $d \gg \lambda_p^2/\lambda_\sigma$. Different regimes can be reached depending on the relative size of length scales: Arrow (1) corresponds to an increasing distance d which ultimately leads to a strictly *nonuniversal* interaction. Arrow (2) indicates an overall increase of the geometry (i.e., d/R_c fixed) with constant conductivity leading to a *universal* interaction.

energy does not depend on the material properties of the objects and is universal [12,13].

Although in a wire-sphere system the Casimir interaction depends on the material properties of the particle at all separations, the signatures of the universal behavior of the metallic wire are still traceable at asymptotic separations. For a plasma wire at intermediate distances, $d/R_c \ll \exp(\lambda_p^2/R_c^2)$, the Casimir interaction depends both on the material properties of the wire and the particle. For larger separations, $d/R_c \gg \exp(\lambda_p^2/R_c^2)$, the interaction is independent of the material properties of the plasma wire, while it still depends on the material properties of the particle [see Fig. 1(a)].

For a Drude wire and a metallic particle, at larger separations, $d^2/R_c^2 \gg d/\lambda_\sigma$, the interaction depends both on the material properties of the Drude wire and that of the spherical particle [see Fig. 1(b)]. At intermediate distances $d^2/R_c^2 \ll d/\lambda_\sigma$, while material properties of the sphere have a significant role in the Casimir energy, it does not depend on the material properties of the wire. Note that the Casimir interaction is also independent of the material properties for two parallel Drude wires [12,13].

IV. INTERMEDIATE-SEPARATION REGIME: NUMERICAL CALCULATIONS

We use Eq. (2) to numerically calculate the Casimir energy. The numerical algorithm consists of three major parts: (i) constructing the matrix $\mathbb{N}$ from Eq. (6), (ii) computing the determinant of $\mathbf{1} - \mathbb{N}$ for specific imaginary frequencies κ, and (iii) integrating over κ. The matrix $\mathbb{N}$ consists of blocks which are associated with the quantum numbers ℓ and ℓ'. We truncate ℓ and ℓ' at a finite partial wave number $\ell_{\max}$ such that the result for the energy changes by less than a factor of 1.0001 upon increasing $\ell_{\max}$ by 1. Since $\ell, \ell' \leqslant \ell_{\max}$, the N matrix has $\ell_{\max}^2$ blocks $N_{\ell\ell'}$. The block $\mathbf{N}_{\ell\ell'}$ consists of the elements $\mathbf{N}_{\ell m,\ell' m'}$ which form 2×2 blocks, with $m = -\ell, \ldots, \ell$ and $m' = -\ell', \ldots, \ell'$,

$$\mathbf{N}_{\ell m,\ell' m'} = \begin{pmatrix} \mathbb{N}^{MM}_{\ell m,\ell' m'} & \mathbb{N}^{ME}_{\ell m,\ell' m'} \\ \mathbb{N}^{EM}_{\ell m,\ell' m'} & \mathbb{N}^{EE}_{\ell m,\ell' m'} \end{pmatrix}.$$

Consequently the size of the block $\mathbf{N}_{\ell\ell'}$ is $(4\ell+2)\times(4\ell'+2)$, implying that the off-diagonal blocks ($\ell \neq \ell'$) are not square matrices. Furthermore, $\mathbf{N}_{\ell\ell'}$ blocks are not diagonal since symmetry along the axis parallel to the wire's axis is broken by the particle.

To construct the matrix $\mathbb{N}$, $4\ell_{\max}^2(\ell_{\max}+2)^2$ integrals over k_z have to be evaluated for each κ. This makes the numerical computations for closer separations quite expensive. For example, at separation $d/R = 2.6$, the energy converges with $\ell_{\max} = 12$, corresponding to a matrix of size 336 with 112 896 k_z integrals for just a single value of κ.

Figure 2 illustrates our numerical results for a metallic cylinder and a metallic spherical particle both with the radius R. The plots show the Casimir energy normalized to the energies for the perfect metal wire-particle configuration as a function of the surface-to-surface distance $h = d - 2R$. For the numerical calculations, we used $\lambda_p/R = 0.05$ and 0.5 with $\lambda_p/\lambda_\sigma = 27.4$, corresponding to the parameters for gold with $\lambda_p = 137$ nm and $\lambda_\sigma \approx 5$ nm [29]. Figure 2 shows the dependence of the Casimir energy on the material properties of the wire and particle. Figure 2(a) depicts the interaction energy between the perfect metal wire with the metallic particle for plasma (open symbols) and Drude (solid symbols) models with $\lambda_p/R = 0.05$ (squares) and 0.5 (circles) and $\lambda_p/\lambda_\sigma = 27.4$. The dashed lines show the asymptotic energies given by Eqs. (26) and (27). As shown in the figure, there is a very good agreement between the asymptotics and the numerical results. The numerical results confirm that at very large separations, only the material properties of the particle contribute to the Casimir energy. We note that in the range of distances considered here and for the parameters of gold, one has to consider the energy given in Eq. (26) in addition to the correction term presented in Eq. (27).

Figure 2(b) shows the interaction between a plasma wire and a perfect metal (open triangles), plasma (open circles), and Drude particles (solid circles) with the plasma wavelength $\lambda_p/R = 0.5$ and $\lambda_p/\lambda_\sigma = 27.4$. The dashed lines show the asymptotic energies given by Eqs. (30) and (31). This figure also shows the good agreement between the asymptotics derived in the previous section and our numerical results. Again, here it is important to include the correction given by Eq. (31). Note that for the perfect metal particle and the

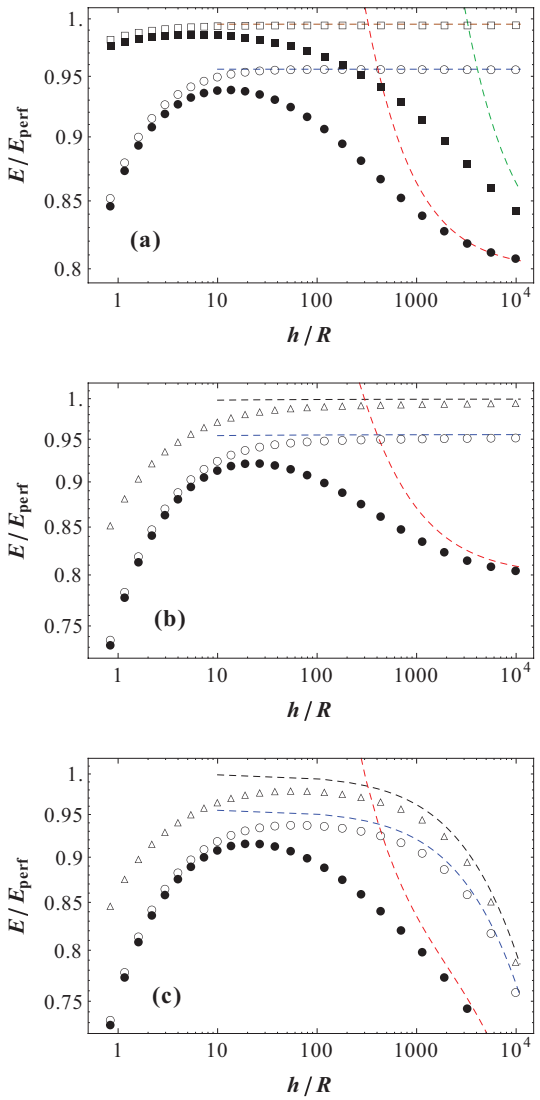

FIG. 2. (Color online) Ratio of the numerically computed energy E for realistic metals to the perfect metal energy $E_{\rm perf}$ vs h/R for a wire and a particle with $R_{\rm c} = R_{\rm s} = R$. Each figure shows the numerics related to a wire with specific material properties: (a) for a perfect metal wire, (b) a plasma wire with $\lambda_{\rm p}/R = 0.5$, and (c) a Drude wire with the same value for $\lambda_{\rm p}/R$ and $\lambda_\sigma = \lambda_{\rm p}/27.4$. The ratio of energies for particles with different material properties are distinguished by different symbols: open triangles for the perfect metal particle and open circles and open squares for plasma particles with $\lambda_{\rm p}/R = 0.5$, 0.05, respectively. Solid circles and solid squares denote Drude particles with $\lambda_{\rm p}/R = 0.5$, 0.05, respectively, and $\lambda_\sigma = \lambda_{\rm p}/27.4$.

plasma cylinder (open triangles) the energy ratio approaches 1 at large separations. This is due to the fact that in this regime the material properties of the plasma wire do not contribute to the Casimir interaction [see Fig. 1(a)].

Figure 2(c) shows the interaction between a Drude wire and a perfect metal (open triangles), a plasma (open circles), and a Drude spherical particles (solid circles) with $\lambda_{\rm p}/R = 0.5$ and $\lambda_{\rm p}/\lambda_\sigma = 27.4$. The dashed lines are obtained by computing the integrals in Eqs. (24) and (25). Since for $10^2 \lesssim d \lesssim 10^4$ we have $10^{-2} \lesssim \xi' \lesssim 10^{-1}$, corresponding to the crossover regime, the asymptotic energies of Eqs. (32) and (33) are not applicable [see Fig. 1(b)].

V. SHORT-SEPARATION REGIME: PROXIMITY FORCE APPROXIMATION

In this section, using the proximity force approximation (PFA) [30], we calculate the Casimir interaction at short separations $h \ll R_{\rm c}, R_{\rm s}$. This method gives the interaction as an integral of the energies between parallel surface segments,

$$\mathcal{E}_{\rm PFA} = \int dA\, E_{\rm plate}(h), \tag{38}$$

where $E_{\rm plate}$ is the Casimir energy per unit area between two parallel plates and h is the surface-to-surface distance. Figure 3 illustrates the distance between two surface elements. According to Fig. 3, the distance h is

$$h = h_0 + R_{\rm s}[1 - \cos(\theta_{\rm s})] + R_{\rm c}[1 - \cos(\phi_{\rm c})], \tag{39}$$

with $h_0 = d - R_{\rm c} - R_{\rm s}$ the distance of the closest approach between the cylinder and the sphere. One can write $\phi_{\rm c}$ in terms of $\theta_{\rm s}$ and $\phi_{\rm s}$,

$$\sin(\phi_{\rm c}) = \frac{R_{\rm s}}{R_{\rm c}} \sin(\theta_{\rm s}) \sin(\phi_{\rm s}). \tag{40}$$

At short separations, the surface elements of the sphere and cylinder in which $\theta_{\rm s} \ll 1$ and $\phi_{\rm c} \ll 1$, respectively, contribute most to the interaction. Therefore, the distance h can be approximated by

$$h(\theta_{\rm s},\phi_{\rm s}) \approx h_0 + \frac{R_{\rm s}\theta_{\rm s}^2}{2}\left(1 + \frac{R_{\rm s}}{R_{\rm c}} \sin^2(\phi_{\rm s})\right). \tag{41}$$

Inserting Eq. (41) into Eq. (38) and performing a simple change of variable, we obtain the PFA energy,

$$\mathcal{E}_{\rm PFA} = \frac{2\pi R_{\rm s}}{\sqrt{1 + \frac{R_{\rm s}}{R_{\rm c}}}} \int_{h_0}^{\infty} dH\, E_{\rm plate}(H). \tag{42}$$

For the case of perfect metal surfaces with $E_{\rm plate}(H)/A = -\pi^2\hbar c/(720H^3)$, we find

$$\mathcal{E}_{\rm PFA} = -\frac{\pi^3 R_{\rm s}\hbar c}{720\sqrt{1 + \frac{R_{\rm s}}{R_{\rm c}}}h_0^2}. \tag{43}$$

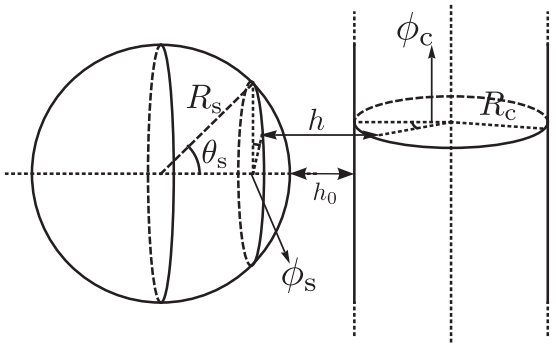

FIG. 3. The geometry of a wire of radius $R_{\rm c}$ and a sphere of radius $R_{\rm s}$ at a distance h_0 (center-to-center distance $d = h_0 + R_{\rm c} + R_{\rm s}$).

For Drude and plasma objects, we use the Lifshitz formula [31],

$$\frac{E_{\rm plane}(h)}{A} = \frac{\hbar c}{(2\pi)^2}\int_0^\infty \kappa^2 d\kappa \int_1^\infty p\,dp \times \ln\left[\left(1-r_{\rm s}^M r_{\rm c}^M e^{-2\kappa p h}\right)\left(1-r_{\rm s}^E r_{\rm c}^E e^{-2\kappa p h}\right)\right], \tag{44}$$

with p a dimensionless variable, and $r_{\rm s}^{M(E)}$ and $r_{\rm c}^{M(E)}$ the Fresnel coefficients of the surface elements for the cylinder and sphere, respectively. The Fresnel coefficients of an object a are given by

$$r_a^M(ic\kappa,p) = \frac{\mu_a(ic\kappa)-\sqrt{1+\left[n_a^2(ic\kappa)-1\right]/p^2}}{\mu_a(ic\kappa)+\sqrt{1+\left[n_a^2(ic\kappa)-1\right]/p^2}},$$
$$r_a^E(ic\kappa,p) = \frac{\epsilon_a(ic\kappa)-\sqrt{1+\left[n_a^2(ic\kappa)-1\right]/p^2}}{\epsilon_a(ic\kappa)+\sqrt{1+\left[n_a^2(ic\kappa)-1\right]/p^2}}, \tag{45}$$

where n_a is the refraction index, $n_a(ic\kappa)=\sqrt{\epsilon(ic\kappa)\mu(ic\kappa)}$.

The PFA energy is obtained using Eqs. (42) and (44) together with the dielectric function of Eq. (8). Figure 4 shows the Casimir energy for a perfect metal (open squares) and plasma model $\lambda_{\rm p}/R = 0.5$ (open circles) normalized to the PFA energy. The energies associated with the Drude model are not shown since they collapse on the data for the plasma model at short separations. Our data show that as the distance between the sphere and the cylinder decreases, the values of the energies become closer to the PFA ones. Note that at short separations the energy converges with larger values of $\ell_{\rm max}$. Since the size of the matrix $\tilde{\mathbb{N}}$ increases quadratically with $\ell_{\rm max}$, the numerical calculation of the Casimir energy becomes extremely costly at short separations. In this work the interaction is calculated up to $h/R = 0.4$.

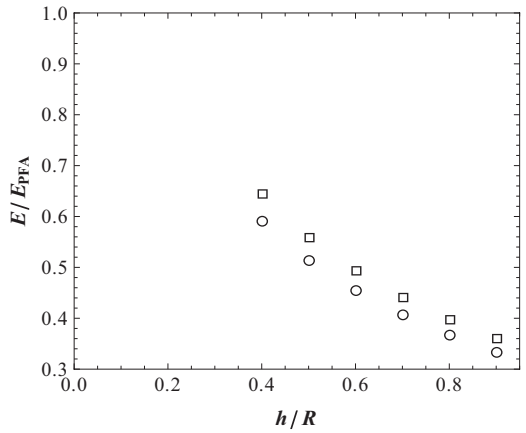

FIG. 4. Ratio of the numerical results for the Casimir energy shown in Fig. 2 and the PFA energy for perfect metals (squares) and for plasma model with $\lambda_{\rm p}/R = 0.5$ (circles). The ratio is shown as a function of surface-to-surface distance h. Similar to Fig. 2, the wire and particle have equal radii $R_{\rm s} = R_{\rm c} = R$.

VI. SUMMARY AND CONCLUSIONS

In summary, we have studied the Casimir energy between a cylindrical wire and a spherical particle. For large separations, we have derived the asymptotic energies for the Drude, plasma, and perfect metal models. In addition, we have calculated the Casimir interaction between a metallic wire and an isotropic atom. Our results for the wire-atom system is in complete agreement with previous results obtained through a different method [25–28].

Furthermore, we have computed the Casimir interaction between a spherical particle and a wire. Such computations are quite demanding due to lack of spherical symmetry. Our numerical results perfectly match the asymptotic energies.

For short separations, we obtained the energy using the proximity force approximation (PFA) and compared it with our numerical data. This comparison indicates that as the distance between the wire and particle decreases, the numerical results for the Casimir energy becomes closer to the PFA one. It is noteworthy that depending on the separation, the material properties of the metallic wire may not play a role in the interaction energy, similar to the parallel wires and wire-plate systems [12,13].

In a cylinder-sphere system, we do not observe a universal behavior as we have previously obtained for parallel wires and a wire-plate geometries because of the physical properties of the spherical particle. However, one can still have "universal" regimes in which the interaction does not depend on the material properties of the metallic wire.

In the case of the plasma wire with the plasma wavelength $\lambda_{\rm p}$ and radius $R_{\rm c}$, at sufficiently large separations, $d/R_{\rm c} \gg \exp(\lambda_{\rm p}^2/R_{\rm c}^2)$, the material properties of the wire do not play any role in the asymptotic interactions between the wire and a particle or an atom.

In contrast for the Drude wire with conductivity σ and the characteristic length $\lambda_\sigma = 2\pi c/\sigma$, at large separations $d^2/R_{\rm c}^2 \gg d/\lambda_\sigma$, the asymptotic energy depends on the material properties of the wire. Quite interestingly, in the opposite limit, $d^2/R_{\rm c}^2 \ll d/\lambda_\sigma$ and $d \gg \lambda_{\rm p}^2/\lambda_\sigma$, the asymptotic interaction becomes independent of the material properties of the Drude wire. The specific behavior of the Drude wires has been explained in Refs. [12,13] in terms of large-scale charge fluctuations.

At the end we emphasize that since simple generic geometries appear in many nano- and micrometer-sized systems, the knowledge of the interaction between a metallic sphere and cylinder could be important for an efficient design of low-dimensional structures.

ACKNOWLEDGMENTS

We thank M. Kardar and U. Mohideen for useful discussions. This work was supported by the NSF through Grant No. DMR-06-45668 (R.Z.) and DARPA Contract No. S-000354 (R.Z. and T.E.). P.R.-L.'s research has been supported by Projects MOSAICO, UCM (Grant No. PR34/07-15859), MODELICO (Comunidad de Madrid), ENFASIS (Grant No. FIS2011-22644, Spanish Government), by MINECO (Spain) Grant No. FIS2012-38866-C05-01, and by the EPSRC under EP/H049797/1.

APPENDIX A: *T* MATRICES

In this Appendix, for completeness, we present the T matrices of a cylinder and a sphere, from Refs. [12,16]. The T matrix of a sphere in spherical vector wave basis is diagonal in the quantum numbers l,m and the electromagnetic polarizations E and M:

$$T^{M}_{\mathrm{s},\ell m} = -\frac{\pi}{2}\frac{\eta I_{l+\frac{1}{2}}(\kappa R)\left[I_{l+\frac{1}{2}}(n\kappa R)+2n\kappa R I'_{l+\frac{1}{2}}(n\kappa R)\right]-nI_{l+\frac{1}{2}}(n\kappa R)\left[I_{l+\frac{1}{2}}(\kappa R)+2\kappa R I'_{l+\frac{1}{2}}(\kappa R)\right]}{\eta K_{l+\frac{1}{2}}(\kappa R)\left[I_{l+\frac{1}{2}}(n\kappa R)+2n\kappa R I'_{l+\frac{1}{2}}(n\kappa R)\right]-nI_{l+\frac{1}{2}}(n\kappa R)\left[K_{l+\frac{1}{2}}(\kappa R)+2\kappa R K'_{l+\frac{1}{2}}(\kappa R)\right]}, \tag{A1}$$

with $n=\sqrt{\epsilon(i\kappa)\mu(i\kappa)}$ and $\eta=\sqrt{\epsilon(i\kappa)/\mu(i\kappa)}$. The T-matrix elements for E multipoles, $T^{E}_{\mathrm{s},\ell m}$, are obtained from Eq. (A1) by interchanging ϵ and μ.

The T-matrix elements of a cylinder with dielectric response $\epsilon(i\kappa)$ and magnetic permeability $\mu(i\kappa)$ are given by

$$T^{EE}_{k_z n} = -\frac{I_n(pR)}{K_n(pR)}\frac{\Delta_2\Delta_3+K^2}{\Delta_1\Delta_2+K^2}, \tag{A2}$$

$$T^{EM}_{k_z n} = -\frac{K}{\sqrt{\epsilon\mu}(pR)^2K_n(pR)^2}\frac{1}{\Delta_1\Delta_2+K^2}, \tag{A3}$$

with $K=[nk_z/(\sqrt{\epsilon\mu}R^2\kappa)](1/p'^2-1/p^2)$ and

$$\Delta_1 = \frac{I'_n(p'R)}{p'RI_n(p'R)}-\frac{1}{\epsilon}\frac{K'_n(pR)}{pRK_n(pR)}. \tag{A4}$$

Note that Δ_2 can be obtained from Eq. (A4) by interchanging ϵ with μ, and Δ_3 can be found by replacing K'_n with I'_n and K_n with I_n in Eq. (A4). Moreover, $T^{MM}_{k_z n}$ can be obtained by replacing ϵ with μ and considering $T^{ME}_{k_z n}=-T^{EM}_{k_z n}$.

APPENDIX B: *T* MATRIX OF A SPHERE IN CYLINDRICAL BASIS

The electromagnetic field far enough outside a sphere can be written in terms of the regular wave function with the electromagnetic polarization P, $|E^{\mathrm{reg}}_{k_z mP}(ic\kappa)\rangle$, the free electromagnetic Green's function $\mathbb{G}_0(ic\kappa)$, and the scattering operator of the sphere $\mathbb{T}_{\mathrm{s}}(ic\kappa)$ [7],

$$|E\rangle = \left|E^{\mathrm{reg}}_{k_z mP}\right\rangle - \mathbb{G}_0\mathbb{T}_{\mathrm{s}}\left|E^{\mathrm{reg}}_{k_z mP}\right\rangle, \tag{B1}$$

where $ic\kappa$ arguments are dropped for brevity. The description of the regular and outgoing wave functions in various bases, including spherical and cylindrical wave bases, is given in Appendix B of Ref. [7].

The expansion of the free Green's function in terms of the regular and outgoing wave functions is given by

$$\mathbb{G}_0 = \sum_{k_z mP} C_P\left|E^{\mathrm{out}}_{k_z mP}\right\rangle\left\langle E^{\mathrm{reg}}_{k_z mP}\right|, \tag{B2}$$

where $C_E=-C_M=1/(2\pi L)$ is the normalization coefficient with L the overall length of the cylinder. Using the cylindrical vector wave functions given in Appendix B of Ref. [7], Eq. (B2) is rewritten as

$$\mathbb{G}_0 = \frac{L}{2\pi}\int dk_z\sum_m C_M\mathbf{M}^{\mathrm{out}}_{k_z m}(\kappa,\mathbf{x})\otimes\mathbf{M}^{\mathrm{reg}*}_{k_z m}(\kappa,\mathbf{x}') + C_E\mathbf{N}^{\mathrm{out}}_{k_z m}(\kappa,\mathbf{x})\otimes\mathbf{N}^{\mathrm{reg}*}_{k_z m}(\kappa,\mathbf{x}'), \tag{B3}$$

where $(\mathbf{M}^{\mathrm{reg}}_{k_z m},\mathbf{N}^{\mathrm{reg}}_{k_z m})$ and $(\mathbf{M}^{\mathrm{out}}_{k_z m},\mathbf{N}^{\mathrm{out}}_{k_z m})$ are the regular and outgoing cylindrical vector wave functions [7]. Equation (B3) holds for $\rho<\rho'$ with ρ the radial component of $\mathbf{x}$.

Inserting Eq. (B2) into Eq. (B1) yields

$$|E\rangle = \left|E^{\mathrm{reg}}_{k'_z m'P'}\right\rangle + \sum_{k_z mP}\left|E^{\mathrm{out}}_{k_z mP}\right\rangle T^{PP'}_{\mathrm{s},k_z m,k'_z m'}, \tag{B4}$$

with

$$T^{PP'}_{\mathrm{s},k_z m,k'_z m'} = (-1)C_P\left\langle E^{\mathrm{reg}}_{k_z mP}\right|\mathbb{T}_{\mathrm{s}}\left|E^{\mathrm{reg}}_{k'_z m'P'}\right\rangle, \tag{B5}$$

the T matrix of a sphere in cylindrical basis. Equation (B4) describes "exterior" scattering, in which the outgoing waves describe the scattered field and the regular waves the incoming field (see Ref. [7]). Note that Eq. (B5) does not depend on the outgoing wave functions due to the fact that we are investigating an "exterior" scattering problem, where the scatterer scatters waves from its outside surface to the free unbounded space.

Now we expand the cylindrical basis wave functions in terms of the spherical basis waves,

$$\left|E^{\mathrm{reg}}_{k_z mP}\right\rangle = \sum_{\ell Q} D_{\ell mQ,k_z mP}\left|E^{\mathrm{reg}}_{\ell mQ}\right\rangle, \tag{B6}$$

where Q is the electromagnetic polarization, ℓ is the quantum number related to the spherical wave functions, and the coefficients $D_{\ell mQ,k_z mP}$ are the elements of the conversion matrix from the cylindrical to spherical basis (see Appendix C for a detailed description). Since the azimuthal dependence of the wave functions on both sides of Eq. (B6) is the same, the sum runs on the quantum number ℓ and polarization Q.

Inserting Eq. (B6) into Eq. (B5), we obtain

$$T^{PP'}_{\mathrm{s},k_z m,k'_z m'} = \sum_{\ell Q,\ell' Q'}\frac{C_P}{C'_Q(\kappa)}D^{\dagger}_{k_z mP,\ell mQ}T^{QQ'}_{\mathrm{s},\ell m,\ell' m'}D_{\ell' m'Q',k'_z m'P'}, \tag{B7}$$

with

$$T^{QQ'}_{\mathrm{s},\ell m,\ell' m'} = (-1)C'_Q(\kappa)\left\langle E^{\mathrm{reg}}_{\ell mQ}\right|\mathbb{T}_{\mathrm{s}}\left|E^{\mathrm{reg}}_{\ell' m'Q'}\right\rangle, \tag{B8}$$

the T matrix of the sphere in the spherical basis (see Appendix A) and $C'_M(\kappa)=-C'_E(\kappa)=\kappa$ the normalization

coefficients of the Green's function expansion in the spherical basis. The ratio of the normalization coefficients in Eq. (B7) is $(1-2\delta_{P,Q})/(2\pi\kappa L)$. Since the T matrix of the sphere in the spherical basis is diagonal in l,m and polarization, Eq. (B7) is simplified to

$$T^{PP'}_{\mathrm{s},k_z m,k'_z m} = \frac{1}{2\pi\kappa L}\sum_{\ell=\max(1,|m|)}^{\infty}\sum_{Q}(1-2\delta_{P,Q}) \times D^{\dagger}_{k_z m P,\ell m Q} T^{Q}_{\mathrm{s},\ell m} D_{\ell m Q,k'_z m P'}. \tag{B9}$$

APPENDIX C: CONVERSION MATRIX $\mathbf{D}_{\ell m,k_z m}$

The coefficients of the expansion of the cylindrical vector waves in terms of the spherical ones determine the elements of the conversion matrix $\mathbf{D}_{\ell m,k_z m}$. These coefficients are known and have already been calculated [32–34]. In this Appendix we make the previously derived coefficients consistent with the Wick-rotated vector wave bases introduced in Ref. [7]. The expansion of cylindrical vector waves $(\mathbf{m}_{m\lambda},\mathbf{n}_{m\lambda})$ in terms of spherical vector waves $(\mathbf{m}_{\ell m},\mathbf{n}_{\ell m})$ is given by Ref. [33]

$$\begin{aligned}\mathbf{m}_{m\lambda} &= \sum_{l=m}^{\infty} A_{\ell m\lambda}\mathbf{m}_{\ell m} + B_{\ell m\lambda}\mathbf{n}_{\ell m},\\ \mathbf{n}_{m\lambda} &= \sum_{l=m}^{\infty} A_{\ell m\lambda}\mathbf{n}_{\ell m} + B_{\ell m\lambda}\mathbf{m}_{\ell m},\end{aligned} \tag{C1}$$

where $\lambda^2 = k^2 - h^2$ and

$$\begin{aligned}A_{\ell m\lambda} &= \frac{2\ell+1}{\ell(\ell+1)}\frac{(\ell-m)!}{(\ell+m)!} i^{\ell-m+1} k \sin(\alpha)\frac{d}{d\alpha}P^m_\ell(\cos(\alpha)),\\ B_{\ell m\lambda} &= \frac{2\ell+1}{\ell(\ell+1)}\frac{(\ell-m)!}{(\ell+m)!} i^{\ell-m+1} m k P^m_l(\cos(\alpha)),\end{aligned} \tag{C2}$$

with $\cos(\alpha) = h/k$. Note that $\mathbf{m}$ and $\mathbf{n}$ are the vector wave functions in Euclidean space.

Taking into account $h \equiv k_z$, $k \equiv i\kappa$, and $\lambda \equiv i\sqrt{\kappa^2+k_z^2}$, the vector wave bases $(\mathbf{M}^{\mathrm{reg}},\mathbf{N}^{\mathrm{reg}})$ defined in Ref. [7] are related to the bases $(\mathbf{m},\mathbf{n})$ defined in Ref. [33] by the relations

$$\begin{aligned}\mathbf{m}_{m\lambda} &= i^m\sqrt{\kappa^2+k_z^2}\,\mathbf{M}^{\mathrm{reg}}_{k_z m}(\kappa,\mathbf{x}),\\ \mathbf{n}_{m\lambda} &= i^{m-1}\sqrt{\kappa^2+k_z^2}\,\mathbf{N}^{\mathrm{reg}}_{k_z m}(\kappa,\mathbf{x}),\end{aligned} \tag{C3}$$

and

$$\begin{aligned}\mathbf{m}_{\ell m} &= i^\ell\sqrt{\frac{4\pi\,\ell(\ell+1)(\ell+m)!}{(2\ell+1)(\ell-m)!}}\mathbf{M}^{\mathrm{reg}}_{\ell m}(\kappa,\mathbf{x}),\\ \mathbf{n}_{\ell m} &= i^{\ell-1}\sqrt{\frac{4\pi\,\ell(\ell+1)(\ell+m)!}{(2\ell+1)(\ell-m)!}}\mathbf{N}^{\mathrm{reg}}_{\ell m}(\kappa,\mathbf{x}).\end{aligned} \tag{C4}$$

Plugging Eqs. (C2) [after a Wick rotation $(k \to i\kappa)$], (C3), and (C4) into Eq. (C1), we obtain

$$\begin{aligned}\mathbf{M}^{\mathrm{reg}}_{k_z m}(\kappa,\mathbf{x}) &= \sum_{l=m}^{\infty} D_{\ell mM,k_z mM}\mathbf{M}^{\mathrm{reg}}_{\ell m}(\kappa,\mathbf{x}) + D_{\ell mE,k_z mM}\mathbf{N}^{\mathrm{reg}}_{\ell m}(\kappa,\mathbf{x}),\\ \mathbf{N}^{\mathrm{reg}}_{k_z m}(\kappa,\mathbf{x}) &= \sum_{l=m}^{\infty} D_{\ell mM,k_z mE}\mathbf{M}^{\mathrm{reg}}_{\ell m}(\kappa,\mathbf{x}) + D_{\ell mE,k_z mE}\mathbf{N}^{\mathrm{reg}}_{\ell m}(\kappa,\mathbf{x}),\end{aligned} \tag{C5}$$

where the conversion matrix elements read

$$\begin{aligned}D_{\ell mM,k_z mM} &= (-1)^{\ell-m}\sqrt{\frac{4\pi(2\ell+1)(\ell-m)!}{\ell(\ell+1)(\ell+m)!}} \times\left(1+\frac{k_z^2}{\kappa^2}\right)^{\frac{1}{2}} P'^m_\ell(-ik_z/\kappa),\\ D_{\ell mE,k_z mM} &= (-1)^{\ell-m}\sqrt{\frac{4\pi(2\ell+1)(\ell-m)!}{\ell(\ell+1)(\ell+m)!}} \times im\left(1+\frac{k_z^2}{\kappa^2}\right)^{-\frac{1}{2}} P^m_\ell(-ik_z/\kappa),\\ D_{\ell mM,k_z mE} &= -D_{\ell mE,k_z mM},\quad D_{\ell mE,k_z mE} = D_{\ell mM,k_z mM}.\end{aligned} \tag{C6}$$

Since it is difficult to deal with the Legendre functions with complex arguments, we use the Rodrigues representation of Legendre polynomials and find

$$P^m_\ell(-ix) = (-i)^{\ell+m} f^m_\ell(x), \tag{C7}$$

where the real function f^m_l is given by

$$f^m_l(x) = \frac{1}{2^\ell \ell!}(1+x^2)^{\frac{m}{2}}\frac{d^{\ell+m}}{dx^{\ell+m}}(1+x^2)^\ell. \tag{C8}$$

Using Eq. (C7), we can write the conversion matrix $\mathbf{D}_{\ell m,k_z m}$ in terms of a modified matrix $\tilde{\mathbf{D}}_{\ell m,k_z m}$,

$$\mathbf{D}_{\ell m,k_z m} = (-1)^{\ell-m}(-i)^{\ell+m-1}\tilde{\mathbf{D}}_{\ell m,k_z m}, \tag{C9}$$

with

$$\begin{aligned}\tilde{D}_{\ell mM,k_z mM} &= \sqrt{\frac{4\pi(2\ell+1)(\ell-m)!}{\ell(\ell+1)(\ell+m)!}} \times\left(1+\frac{k_z^2}{\kappa^2}\right)^{\frac{1}{2}} f^{m\prime}_\ell(k_z/\kappa),\\ \tilde{D}_{\ell mE,k_z mM} &= \sqrt{\frac{4\pi(2\ell+1)(\ell-m)!}{\ell(\ell+1)(\ell+m)!}} \times m\left(1+\frac{k_z^2}{\kappa^2}\right)^{-\frac{1}{2}} f^m_\ell(k_z/\kappa),\\ \tilde{D}_{\ell mM,k_z mE} &= -\tilde{D}_{\ell mE,k_z mM},\quad \tilde{D}_{\ell mE,k_z mE} = \tilde{D}_{\ell mM,k_z mM}.\end{aligned} \tag{C10}$$

[1] *Casimir Physics*, edited by D. Dalvit, P. Milonni, D. Roberts, and F. Rosa, Lecture Notes in Physics, Vol. 834 (Springer, Berlin, 2011).

[2] O. Kenneth and I. Klich, Phys. Rev. Lett. **97**, 160401 (2006).

[3] F. M. Serry, D. Walliser, and G. J. Maclay, Br. J. Appl. Phys. **84**, 2501 (1998).

[4] S. J. Rahi, M. Kardar, and T. Emig, Phys. Rev. Lett. **105**, 070404 (2010).

[5] M. Kardar and R. Golestanian, Rev. Mod. Phys. **71**, 1233 (1999).
[6] M. Bordag, G. L. Klimchitskaya, U. Mohideen, and V. M. Mostepanenko, *Advances in the Casimir Effect* (Oxford University Press, Oxford, UK, 2009).
[7] S. J. Rahi, T. Emig, N. Graham, R. L. Jaffe, and M. Kardar, Phys. Rev. D **80**, 085021 (2009).
[8] A. Lambrecht, P. A. Maia Neto, and S. Reynaud, New J. Phys. **8**, 243 (2006).
[9] M. F. Maghrebi, S. J. Rahi, T. Emig, N. Graham, R. L. Jaffe, and M. Kardar, Proc. Natl. Acad. Sci. USA **108**, 6867 (2011).
[10] N. Graham, A. Shpunt, T. Emig, S. J. Rahi, R. L. Jaffe, and M. Kardar, Phys. Rev. D **81**, 061701 (2010).
[11] T. Emig, N. Graham, R. L. Jaffe, and M. Kardar, Phys. Rev. A **79**, 054901 (2009).
[12] E. Noruzifar, T. Emig, and R. Zandi, Phys. Rev. A **84**, 042501 (2011).
[13] E. Noruzifar, T. Emig, U. Mohideen, and R. Zandi, Phys. Rev. B **86**, 115449 (2012).
[14] T. Emig, R. L. Jaffe, M. Kardar, and A. Scardicchio, Phys. Rev. Lett. **96**, 080403 (2006).
[15] S. J. Rahi, T. Emig, R. L. Jaffe, and M. Kardar, Phys. Rev. A **78**, 012104 (2008).
[16] R. Zandi, T. Emig, and U. Mohideen, Phys. Rev. B **81**, 195423 (2010).
[17] A. Lambrecht and V. N. Marachevsky, Phys. Rev. Lett. **101**, 160403 (2008).
[18] H.-C. Chiu, G. L. Klimchitskaya, V. N. Marachevsky, V. M. Mostepanenko, and U. Mohideen, Phys. Rev. B **81**, 115417 (2010).
[19] H.-C. Chiu, G. L. Klimchitskaya, V. N. Marachevsky, V. M. Mostepanenko, and U. Mohideen, Phys. Rev. B **80**, 121402 (2009).
[20] V. Marachevsky, J. Phys. A: Math. Theor. **45**, 374021 (2012).
[21] H. B. G. Casimir and D. Polder, Phys. Rev. **73**, 360 (1948).
[22] F. Arnecke, H. Friedrich, and P. Raab, Phys. Rev. A **78**, 052711 (2008).
[23] J. Denschlag, G. Umshaus, and J. Schmiedmayer, Phys. Rev. Lett. **81**, 737 (1998).
[24] M. Bawin and S. A. Coon, Phys. Rev. A **63**, 034701 (2001).
[25] Y. Barash and A. Kyasov, Sov. Phys. JETP **68**, 39 (1989).
[26] C. Eberlein and R. Zietal, Phys. Rev. A **75**, 032516 (2007).
[27] C. Eberlein and R. Zietal, Phys. Rev. A **80**, 012504 (2009).
[28] V. B. Bezerra, E. R. Bezerra de Mello, G. L. Klimchitskaya, V. M. Mostepanenko, and A. A. Saharian, Eur. Phys. J. C **71**, 1614 (2011).
[29] R. S. Decca, D. López, E. Fischbach, G. L. Klimchitskaya, D. E. Krause, and V. M. Mostepanenko, Phys. Rev. D **75**, 077101 (2007).
[30] B. V. Derjaguin, Kolloid Z. **69**, 155 (1934).
[31] E. M. Lifshitz, Sov. Phys. JETP **2**, 73 (1956).
[32] S. N. Samaddar, in *Proceedings of the 1971 International Symposium on Antennas Propagation, Sendai, Japan* (IEICE, Tokyo, 1971), p. 195.
[33] R. J. Pogorzelski and E. Lun, Radio Sci. **11**, 753 (1976).
[34] G. Han, Y. Han, and H. Zhang, J. Opt. A: Pure Appl. Opt. **10**, 015006 (2008).